Pro-oxidant Activity of Aluminum: Stabilization of the Aluminum Superoxide Radical Ion

ARTICLE *in* THE JOURNAL OF PHYSICAL CHEMISTRY A · JUNE 2011

Impact Factor: 2.69 · DOI: 10.1021/jp203290b

THE JOURNAL OF PHYSICAL CHEMISTRY A

ARTICLE

pubs.acs.org/JPCA

Pro-oxidant Activity of Aluminum: Stabilization of the Aluminum Superoxide Radical Ion

J. I. Mujika,*[,†] F. Ruipérez,[†] I. Infante,[†] J. M. Ugalde,[†] C. Exley,[‡] and X. Lopez[†]

[†]Kimika Fakultatea, Euskal Herriko Unibertsitatea, and Donostia International Physics Center (DIPC), P.K. 1072, 20080 Donostia, Euskadi, Spain

[‡]Birchall Centre for Inorganic Chemistry and Materials Science, Keele University, Staffordshire, U.K.

Supporting Information

ABSTRACT: The pro-oxidant activity of aluminum, a nonredox metal, through superoxide formation is studied by theoretical methods, determining the ESR **g**-tensor values of $O_2^{\bullet-}$ with a variety of metals and the reaction energies for Al^{3+} superoxide affinity in solution. First, the intrinsic ability of aluminum to induce a splitting of the π_g levels is compared to that of other significant biological metals, such as Na^+, K^+, Mg^{2+}, and Ca^{2+}. Additional properties such as bond lengths, ionization potentials, and electron affinities are also determined, and the coherency with the trends observed from ESR **g**-tensor values is analyzed. As it corresponds to the high charge and its small size, there is a strong interaction between Al^{3+} and the superoxide. We predict that this strong inherent interaction remains when aluminum is microsolvated. Finally, we analyze the possibility of Al^{3+} superoxide formation in solution, leading to the conclusion that substitution of the first coordination shell water molecules is plausible, but not of hydroxides. This points to the possibility of Al^{3+} superoxide formation in solution, which would be pH-dependent. Taking into account the earlier established linear relationship between metal−superoxide interactions and promoting effects in electron-transfer reactions, our work reinforces the idea that the presence of aluminum in biological systems could lead to an important pro-oxidant activity through a superoxide formation mechanism.

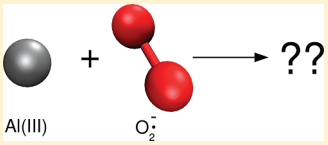

1. INTRODUCTION

Aluminum is the most abundant metal in the earth's crust but has largely been excluded from biochemical evolution by its efficient cycling within the lithosphere.[1,2] However, human intervention (soil acidification, food additives, pharmaceuticals, aluminum containers, etc.) has increased the availability of biologically reactive aluminum,[2,3] and its presence has been linked to various human diseases.[4−6] The exact mechanisms for aluminum toxicity are still unknown, but a first step toward their understanding lies on the characterization of aluminum speciation in biosystems.

Aluminum is able to form a high variety of strong complexes with diverse bioligands, including high molecular mass (HMM) proteins such as transferrin[7] and low molecular mass (LMM) molecules such as citrate.[8,9] The characterization of Al(III) speciation in biosystems is a complex problem, and theoretical calculations can help shed light on the different Al(III) complexes formed in aqueous solution at equilibrium[8−19] and nonequilibrium.[20,21] Moreover, model calculations show[9,15,22] that the structural and chemical properties of the ligands can be deeply altered when bound to Al^{3+}, indicating an important interference in biological systems when Al^{3+} is introduced. In addition, Al^{3+} can displace[3,4,11−13,15,23] essential metal cofactors (particularly Mg^{2+}) in proteins, producing malfunctions of the affected metalloproteins. Additional reported bioeffects of Al(III) include interaction with phosphates such as ADP and ATP[3] and enhancement of reactive oxygen species (ROS) production.[5]

Aluminum exhibits a significant pro-oxidant activity, promoting biological oxidation both in vitro and in vivo.[24,25] The existence of an Al^{3+} superoxide complex has been hypothesized[26] to be central to this oxidant activity. In this vein, Fukuzumi et al.[27−29] have shown that there exists a linear relationship between the oxidant activity of a number of metals and the interaction strength with the superoxide anion. This strength can be accurately estimated by measuring the electron spin resonance (ESR) **g**-tensor in metal superoxide complexes,[27−29] and hence, this quantity can be taken as a reliable indicator of the pro-oxidant activity of a given metal in biosystems.

In the present paper, we study the affinity of aluminum toward the superoxide anion by a variety of theoretical methods. First, we determine the ESR **g**-tensor value by highly accurate theoretical methods for several biologically relevant, gas-phase metal superoxide complexes (M = Na^+, K^+, Mg^{2+}, Ca^{2+}), and then, we compare them with the same value for aluminum. The purpose of these calculations is to determine the inherent strength of aluminum−superoxide interactions. We show that aluminum has an intrinsic high potential to stabilize a superoxide anion. Later, we re-evaluate these quantities for selected metals (Mg^{2+}, Ca^{2+}, Al^{3+}) in a number of microsolvated structures and demonstrate that, even if the aluminum−superoxide interaction is modulated in microsolvated environments, it is still significantly higher than the one displayed by other metals that are prone to Al^{3+} exchange. Finally, the possibility of Al^{3+} superoxide formation

Received: April 8, 2011
Revised: May 6, 2011
Published: May 23, 2011

in solution is discussed in terms of the calculated reaction free energies for superoxide displacement of first coordination shell water/hydroxide ligands. We observed that an Al^{3+} superoxide complex might be formed by displacement of a water molecule from the first solvation shell of Al(III) in an aqueous solution. Our calculations point to Al^{3+} species as the main route toward the formation of superoxide complexes in water.

2. METHODS SECTION

A. Geometry Optimizations. All geometrical optimizations were carried out in gas phase using the Gaussian 09[30] suite of programs employing the B3LYP functional[31−34] in conjunction with the 6-31++g(d,p) basis set. To confirm that the optimized structures were minima on the potential energy surfaces, frequency calculations were done at the same level of theory. All structures showed real frequencies for all of the normal modes of vibration. The frequencies were then used to evaluate the zero-point vibrational energy (ZPVE) and the thermal (T = 298 K) vibrational corrections to the enthalpy and Gibbs free energy in the harmonic oscillator approximation. To calculate the entropy, the different contributions to the partition function were evaluated using the standard expressions for an ideal gas in the canonical ensemble and the harmonic oscillator and rigid rotor approximations. The electronic energy was refined by single-point energy calculations at the B3LYP/6-311++G(3df,2p) level of theory. Single-point calculations were also perfomed with PBE0[35] and M06-2X[36] levels of theory, in order to assess the adequacy of the B3LYP functional to evaluate reaction energies for substitution of OH_2/OH^- by the $O_2^{\bullet-}$ superoxide calculated at the first coordination shell of the Al^{+3} hydrolysis species. These calculations demonstrate the satisfactory performance of the B3LYP functional, and therefore, this functional will be the only one included in the text hereafter. The comparison among the three functionals might be found in the Supporting Information.

B. CASSCF and CASPT2 Calculations. Wave-function-based calculations were performed at the second-order Douglas−Kroll−Hess Hamiltonian all-electron level of theory.[37,38] The wave functions were obtained by means of complete active space self-consistent field calculations (CASSCF),[39−41] where the active space is defined by eight molecular orbitals from the $O_2^{\bullet-}$ unit, σ_{2s}, σ_{2s}^*, σ_{2p_z}, π_{2p_x}, π_{2p_y}, $\pi_{2p_x}{}^*$, $\pi_{2p_y}{}^*$, and $\sigma_{2p_z}{}^*$, and one ns orbital from the metal. In these 9 orbitals, we distributed 13 electrons. Dynamic correlation is taken into account through complete active space second-order perturbation theory calculations (CASPT2).[42,43] The imaginary shift technique[44] was used to achieve convergence and avoid the presence of intruder states in the CASPT2 step, where the inner $(n-1)$s and $(n-1)$p orbitals from the metals, as well as all the water molecules molecular orbitals (excluding the oxygen 1s orbitals), are also correlated dynamically. The value of the shift employed in this work was 0.20 au. All CASSCF/CASPT2 calculations were performed with the MOLCAS 7.4 suite of programs.[45] There are two approaches to calculate **g**-tensors;[46] the first one treats spin−orbit coupling and the Zeeman effect simultaneously by using second-order perturbation theory, and the second one adds the Zeeman effect through first-order perturbation theory within the ground-state Kramers doublet. This second approach, which is limited to systems with an isolated Kramers doublet, so that the Zeeman effect can be safely treated only within this doublet, is the one used in this work. The calculation of the **g**-tensors is carried out using the RASSI module included in the MOLCAS package.

Table 1. Gas-Phase B3LYP/6-31++G(d,p) Geometries of $M^{n+}O_2^{\bullet-}$ Complexes[a]

M^{n+}	O−O	M−O	∠M−O−O
Na^+	1.356	2.141	71.5
K^+	1.351	2.476	74.2
Mg^{2+}	1.378	1.914	68.9
Ca^{2+}	1.358	2.228	72.2
Al^{3+}	1.437	1.774	66.1

[a] Distances are in Å, and angles are in degrees.

We have used the all-electron atomic natural orbitals (ANO-RCC) basis sets of quadruple-ζ size for all atoms, with the following primitives and contractions: on aluminum, (17s12p5d3f2g)/[6s5p3d2f];[47] on sodium, (17s12p5d4f2g)/[6s5p3d2f];[48] on magnesium, (17s12p6d2f2g)/[7s4p4d2f];[48] on potassium, (21s16p5d4f2g)/[7s6p3d2f];[48] on calcium, (20s16p6d4f2g)/[8s5p4d2f];[48] on oxygen, (14s9p4d3f2g)/[5s4p3d2f];[47] and finally, on hydrogen, (8s4p3d1f)/[4s3p2d].[49]

C. Bulk Solvent Effects. Two alternative procedures were followed to estimate the solvation free energies of the gas-phase B3LYP/6-31++G(d,p) geometries and using the self-consistent reaction field (SCRF) method. In the first one, denoted as ΔG_{aq}^{PCM}, the polarizable continuum model (PCM) approach[50−53] was employed using the united atom Hartree−Fock (UAHF) set of atomic radii to build the cavity. These radii have been optimized with the HF/6-31G(d) wave function to give accurate solvation free energies of a data set of anionic/cationic and neutral organic and inorganic molecules.[51] Therefore, the HF/6-31G(d) level of theory was chosen to represent the solute. In the second one, ΔG_{aq}^{SMD}, the solvation model density (SMD), a universal solvation model developed by Truhlar et al.,[54] was employed at the B3LYP/6-311++g(3df,2p) level of theory.

Thus, the final free energy in aqueous solvent (G_{aq}) for each structure was evaluated as

$$G_{aq} = E_{electr} + ZPVE + E^{therm} - T\cdot S + \Delta G_{solv}$$

where E_{electr} stands for the B3LYP/6-311++G(3dp,2p) electronic energy in the gas phase, ZPVE the zero-point vibrational energy, E^{therm} the thermal energy contribution, and $T\cdot S$ the entropy contribution at 298 K; ΔG_{solv}, the solvation free energy, is determined with either PCM or SMD.

3. RESULTS AND DISCUSSION

A. Gas-Phase Data. The main geometrical parameters of the $M^{n+}O_2^{\bullet-}$ complexes can be found in Table 1. All of the complexes display a T-shape structure. The largest M−O distance corresponds to K^+, 2.476 Å, and the shortest corresponds to Al^{3+}, 1.774 Å. As expected, the shorter the M−O distance, the larger the O−O bond length. $Al^{3+}O_2^{\bullet-}$ presents the longest O−O bond length, 1.437 Å, and $K^+O_2^{\bullet-}$ presents the shortest, 1.351 Å.

The deviation of the value of the g_{zz} component of the ESR **g**-tensor from the free electron spin value (g_e = 2.0023) has been proposed[27−29] as a measure of the strength of the $M^{n+}-O_2^{\bullet-}$ interaction. The value of g_{zz} can be related to the energy splitting of the π_g levels of $O_2^{\bullet-}$ ($\Delta\varepsilon_{\pi g}$) by the following simple relation: $g_{zz} = g_e + 2\lambda/\Delta\varepsilon_{\pi g}$, for $\Delta\varepsilon_{\pi g} \gg \lambda$, where λ is the spin−orbit coupling constant of oxygen, namely, 0.014 eV. The larger the interaction of the metal with the superoxide, the larger the splitting of the π_g levels. In Table 2, the calculated g_{zz} and $\Delta\varepsilon_{\pi g}$

Table 2. g-Tensor and Energy Splitting of the π_g Levels of $O_2^{\bullet-}$ ($\Delta\varepsilon_{\pi g}$) of $M^{n+}O_2^{\bullet-}$ in eV, Calculated at the CASPT2 Level of Theory

M^{n+}	g_{zz}		$\Delta\varepsilon_{\pi g}$	
	CASPT2	exp.	CASPT2	exp.
Na^+	2.0823	2.0841	0.35	0.34
K^+	2.0915		0.31	
Mg^{2+}	2.0453	2.0451	0.65	0.65
Ca^{2+}	2.0525	2.0499	0.56	0.58
Al^{3+}	2.0275		1.11	

Table 3. IPs of $[M^{n+}O_2^{\bullet-}]$ Complexes and EAs of $[M^{n+}O_2]$, in eV, Calculated at the CASPT2 Level of Theory

M^{n+}	IP	EA[a]
Na^+	7.3	4.9
K^+	6.8	4.1
Mg^{2+}	15.6	13.5
Ca^{2+}	13.9	11.0
Al^{3+}	25.5	25.1

[a] The spin multiplicity of the ground state for $[M^{n+}O_2]$ complexes is triplet, except for $[Al^{3+}O_2]$ which is a singlet.

values for the $M^{n+}O_2^{\bullet-}$ complexes studied in this work can be found. There is an outstanding agreement between theoretical and available experimental data, although one should take into account that the experiments were conducted in acetonitrile at low temperature and our results are based on gas-phase calculations. We observe that the larger the positive charge and the smaller the size of the metal ion, the lower the value of g_{zz} and the larger the splitting of π_g levels, trends that are coherent with those determined by Fukuzumi et al.[27−29] Regarding Al^{3+}, this metal yields the largest splitting in π_g levels, 1.11 eV, indicating the strongest interaction with the superoxide. The splitting is even larger than the maximum one reported experimentally, namely, 1.00 eV for the $Sc^{3+}O_2^{\bullet-}$ complex.[28]

Additional indications of the stability for metal superoxide complexes are the vertical ionization potential (IP) at geometries of $[M^{n+}O_2^{\bullet-}]$ complexes and the electron affinity (EA) of $[M^{n+}O_2]$ compounds. Large values of these two quantities are indicative of a strong stabilization of the superoxide by its interaction with the metal. In Table 3 are displayed the values obtained in this work. The trends in IPs and EAs confirm the analysis based on **g**-tensor values, obtaining the largest IPs and EAs for metals with larger charge and smaller volume. Nevertheless, the charge seems to be the dominating factor over volume, and aluminum complexes present the largest stabilization of the superoxide with values of IP and EA that are almost twice those of divalent metals.

In summary, geometrical data, ESR **g**-tensor values, IPs, and EAs point to a strong interaction between aluminum and the superoxide anion, much larger than the interaction of other metal ions, and lends support to the hypothesis[26] of the formation of an oxidizing complex between aluminum and superoxide.

B. Microsolvated Structures. To further investigate the possibility of aluminum−superoxide interaction in biological environments, we have studied a variety of microsolvated $M^{n+}O_2^{\bullet-}$ structures (M^{n+} = Ca^{2+}, Mg^{2+}, Al^{3+}). In biological environments,

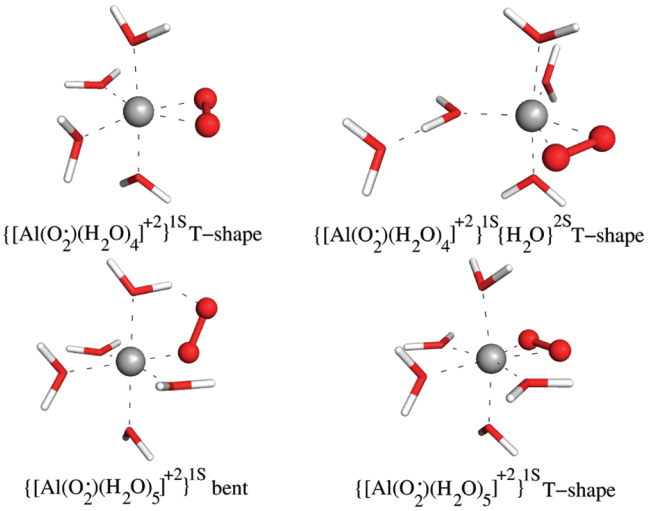

Figure 1. B3LYP/6-31++G(d,p) microsolvated structures for $[AlO_2^{\bullet}]^{2+}$ species.

aluminum is coordinated to water molecules in the first solvation layer, and because of the large charge transfer from these water molecules to aluminum, its effective charge and interaction with the superoxide could be significantly reduced in bioenvironments, resulting in a more similar interaction as compared to other biometals.

1. Coordination Mode. In Table 4, the relative energies of complexes formed by aluminum, magnesium, and calcium with superoxide can be found. Three possible binding modes of $O_2^{\bullet-}$ were analyzed (T-shape, bent, and linear), and the coordination of the metal was completed by four or five water molecules, $[M^{n+}O_2^{\bullet-}](H_2O)_4{}^{1S}$ and $[M^{n+}O_2^{\bullet-}](H_2O)_5{}^{1S}$ models (1S stands for first shell). Additionally, in order to compare the energetics of these two coordination spheres, a $[M^{n+}O_2^{\bullet-}](H_2O)_4{}^{1S}(H_2O)^{2S}$ complex was also considered, with one water molecule in the second solvation shell. Not all of these formal complexes and coordination modes were stable in the optimization procedure, and some of them collapsed to other type of structures (see Figure 1 for the stable structures in the case of $[AlO_2^{\bullet}]^{2+}$ species). For instance, we have not found any stable linearly coordinated complex between the metal and the superoxide. In Table 4, a concise summary of these results is shown. The T-shape binding mode favors a four-water coordination sphere around the metal, whereas the bent binding mode favors five waters in the first coordination shell. In general, T-shape interaction modes are preferred, although the differences in energy are very low. Nevertheless, the tendency toward the T-shape binding mode is more marked for Al^{3+}, with the T-shape $[Al^{3+}O_2^{\bullet-}](H_2O)_4{}^{1S}(H_2O)^{2S}$ complex showing the lowest energy. For Mg^{2+}, the energy differences among the structures are smaller. The T-shape $[Mg^{2+}O_2^{\bullet-}](H_2O)_4{}^{1S}(H_2O)^{2S}$ complex displays the lowest energy at B3LYP, with $[Mg^{2+}O_2^{\bullet-}](H_2O)_5{}^{1S}$ only 0.4 kcal/mol higher in energy. However, at CASPT2, the bent $[Mg^{2+}O_2^{\bullet-}](H_2O)_4{}^{1S}(H_2O)^{2S}$ has the lowest energy, followed by the T-shape $[Mg^{2+}O_2^{\bullet-}](H_2O)_4{}^{1S}(H_2O)^{2S}$. Finally, for Ca^{2+}, we find that the lowest-energy structure is a T-shape $[Ca^{2+}O_2^{\bullet-}](H_2O)_5{}^{1S}$. Probably, due to its bigger size, Ca^{2+} can accommodate a bent/bidentate interaction with $O_2^{\bullet-}$ while keeping five waters in the first solvation sphere.

In summary, there is an overall tendency toward T-shape binding modes between the metal and superoxide in these microsolvated

dx.doi.org/10.1021/jp203290b |J. Phys. Chem. A 2011, 115, 6717–6723

Table 4. Relative Energies (in kcal/mol) of Complexes Formed by Aluminum, Magnesium, and Calcium with Superoxide $O_2^{\bullet -}$[a]

complex	T-shape		bent	
	DFT	CASPT2	DFT	CASPT2
Calcium				
$\{[Ca(O_2^{\bullet})(H_2O)_4]^+\}^{1S}$		b		b
$\{[Ca(O_2^{\bullet})(H_2O)_4]^+\}^{1S}\{H_2O\}^{2S}$	1.1	3.2		c
$\{[Ca(O_2^{\bullet})(H_2O)_5]^+\}^{1S}$	0.0	0.0	3.4	4.6
Magnesium				
$\{[Mg(O_2^{\bullet})(H_2O)_4]^+\}^{1S}$		b		b
$\{[Mg(O_2^{\bullet})(H_2O)_4]^+\}^{1S}\{H_2O\}^{2S}$	0.0	7.0	2.4	0.0
$\{[Mg(O_2^{\bullet})(H_2O)_5]^+\}^{1S}$	5.4	12.1	0.4	8.9
Aluminum				
$\{[Al(O_2^{\bullet})(H_2O)_4]^{2+}\}^{1S}$		b		b
$\{[Al(O_2^{\bullet})(H_2O)_4]^{2+}\}^{1S}\{H_2O\}^{2S}$	0.0	0.0		b
$\{[Al(O_2^{\bullet})(H_2O)_5]^{2+}\}^{1S}$	10.9	7.9	4.6	3.5

[a] The optimizations were carried out at the B3LYP/6-31++G(d,p) level of theory, and the energies were evaluated by B3LYP/6-311++G-(3df,2p) and CASPT2 single-point calculations using the ANO-RCC basis sets of quadruple-ζ size for all atoms. [b] Converges to the T-shape structure. [c] Converges to $\{[Ca(O_2^{\bullet})(H_2O)_5]^+\}^{1S}$.

structures, which, in the case of smaller ions, especially Al^{3+}, leads to coordination spheres formed by the bidentate superoxide and four water molecules in the first solvation layer. It does not escape our attention that this overall preference for bidentate T-shape structures might be driven by the extra stabilization gained by the formation of the strong hydrogen bond between the waters of the second and first solvation spheres. However, monodentate bent binding modes with five water molecules in the first solvation layer are reasonably close in energy.

*2. **g**-Tensor Values.* In Table 5, the values of g_{zz} and $\Delta\varepsilon_{\pi g}$ for the most relevant microsolvated structures are displayed. As expected, the splittings caused in the superoxide π_g levels by metal interaction are smaller than the ones evaluated in the gas phase, consistent with a donation of electronic charge from the solvation layer to the metal. However, there is still a large differential interaction between Al^{3+} and $O_2^{\bullet -}$, in comparison with other metals. The values of $\Delta\varepsilon_{\pi g}$ for $[Al^{3+}O_2^{\bullet -}]$, 0.62−0.86 eV, are twice as large as those for $[Mg^{2+}O_2^{\bullet -}]$, 0.32−0.42 eV. The splitting of π_g levels is also sensitive to the binding mode between the metal and the superoxide and to the number of water molecules in the solvation sphere, but this effect is relatively small compared to the nature of the metal itself and, in particular, to its formal charge.

C. Displacement of OH^-/H_2O by $O_2^{\bullet -}$. In the previous sections, we have shown evidence for an intrinsic high affinity of aluminum toward $O_2^{\bullet -}$ superoxide. However, an analysis of the formation of an aluminum superoxide complex in aqueous solution should consider the capacity of the superoxide to displace one of the first coordination shell water/hydroxide ligands around any of the Al^{3+} cations. Hence, we have chosen to analyze the reaction free energies for a series of substitution reactions with Al^{3+} hydrolytic species. The aqueous phase has been considered by a supermolecule approach,[14] which introduces a number of explicit water molecules in the calculation and a continuum model to account for bulk solvent effects. First,

Table 5. g_{zz} and $\Delta\varepsilon_{\pi g}$ Values, in eV, for Microsolvated $M^{n+}O_2^{\bullet -}$ Complexes, Calculated at the CASPT2 Level of Theory

complex	g_{zz}	$\Delta\varepsilon_{\pi g}$
Calcium		
$\{[Ca(O_2^{\bullet})(H_2O)_4]^+\}^{1S}$ T-shape	2.0943	0.30
$\{[Ca(O_2^{\bullet})(H_2O)_4]^+\}^{1S}\{H_2O\}^{2S}$ T-shape	2.0890	0.33
$\{[Ca(O_2^{\bullet})(H_2O)_5]^+\}^{1S}$ bent	2.0866	0.33
$\{[Ca(O_2^{\bullet})(H_2O)_5]^+\}^{1S}$ T-shape	2.1142	0.25
Magnesium		
$\{[Mg(O_2^{\bullet})(H_2O)_4]^+\}^{1S}$ T-shape	2.0688	0.42
$\{[Mg(O_2^{\bullet})(H_2O)_4]^+\}^{1S}\{H_2O\}^{2S}$ bent	2.0780	0.37
$\{[Mg(O_2^{\bullet})(H_2O)_4]^+\}^{1S}\{H_2O\}^{2S}$ T-shape	2.0682	0.42
$\{[Mg(O_2^{\bullet})(H_2O)_5]^+\}^{1S}$ bent	2.0696	0.42
$\{[Mg(O_2^{\bullet})(H_2O)_5]^+\}^{1S}$ T-shape	2.0898	0.32
Aluminum		
$\{[Al(O_2^{\bullet})(H_2O)_4]^{2+}\}^{1S}$ T-shape	2.0350	0.86
$\{[Al(O_2^{\bullet})(H_2O)_4]^{2+}\}^{1S}\{H_2O\}^{2S}$ T-shape	2.0375	0.80
$\{[Al(O_2^{\bullet})(H_2O)_5]^{2+}\}^{1S}$ bent	2.0406	0.73
$\{[Al(O_2^{\bullet})(H_2O)_5]^{2+}\}^{1S}$ T-shape	2.0472	0.62

we calibrate our methodology with respect to known experimental data on relative pK_a constants, and then, we analyze the substitution reaction free energies.

1. Calibration of the Method. The performance of our computational methodology has been tested using the following equilibrium

$$OOH^{\bullet} + OH^- \rightarrow O_2^{\bullet -} + H_2O$$

whose reaction free energy can be estimated from the experimental values of the pK_a for $OOH^{\bullet}$ (4.8) and H_2O (15.74). Namely, at room temperature (T = 298 K)

$$\Delta G(T) = 2.303 \times RT(pK_a^{OOH^{\bullet}} - pK_a^{H_2O}) = -14.9 \text{ kcal/mol}$$

Our theoretical results for this reaction are shown in Table 6, using two different continuum models, SMD and PCM at the HF/6-31G* level of theory (see the Methods Section). A value of −24.5 kcal/mol is obtained at the SMD level of theory and −6.5 kcal/mol at PCM. These values bracket the experimental one but show an absolute error of around 10 kcal/mol. The reason for this discrepancy is the difference in the solvation energy of the hydroxide ion, −94.2 kcal/mol at SMD and −111.7 kcal/mol at the PCM level of theory, with the experimental value,[55,56] −105.0 kcal/mol, lying in between. This is not surprising because the evaluation of the solvation energy for anions of small size is delicate for continuum models.[55,56] The inclusion of explicit water molecules in the calculation can help in reducing these errors, and hence, two explicit water molecules interacting with the superoxide/hydroxide anions were introduced in our models. This mixed explicit water/continuum model causes a very significant improvement of the energetics, with values of −18.6 (SMD) and −11.0 kcal/mol (PCM). Further use of this model to solvate neutral species leads only to a slight improvement in the energies, −17.6 (SMD) and −12.6 kcal/mol (PCM). Consequently, two explicit water molecules will be included for the solvation of hydroxide/superoxide/water molecules in the substitution reactions.

Table 6. Relative Acidity of $OOH^{\bullet}$ with Respect to H_2O, Estimated at the B3LYP Level of Theory (see section 2A)

	ΔG_{gas}	ΔG_{aq}^{SMD}	ΔG_{aq}^{PCM}
$OOH^{\bullet} + OH^- \rightarrow O_2^{\bullet -} + H_2O$	−38.3	−24.5	−6.5
$OOH^{\bullet} + OH^-(H_2O)_2 \rightarrow O_2^{\bullet -}(H_2O)_2 + H_2O$	−25.4	−18.6	−11.0
$OOH^{\bullet}(H_2O)_2 + OH^-(H_2O)_2 \rightarrow O_2^{\bullet -}(H_2O)_2 + H_2O(H_2O)_2$	−23.1	−17.6	−12.6

Table 7. B3LYP Reaction Free Energies (see section 2A), in kcal/mol, for Substitution of OH_2/OH^- by $O_2^{\bullet -}$ Superoxide at the First Coordination Shell of Al^{+3} Hydrolysis Species[a]

			first coordination shell waters			first and second coordination shell waters		
			ΔG_{gas}	ΔG_{aq}^{SMD}	ΔG_{aq}^{PCM}	ΔG_{gas}	ΔG_{aq}^{SMD}	ΔG_{aq}^{PCM}
$[Al(H_2O)_6]^{+3} + O_2^{\bullet -}$	→	$[Al(O_2^{\bullet})(H_2O)_5]^{2+} + H_2O$	−288.1	−10.0	11.4	−210.7	−8.3	−15.2
$[Al(OH)(H_2O)_5]^{+2} + O_2^{\bullet -}$	→	$[Al(O_2^{\bullet})(OH)(H_2O)_4]^{+} + H_2O$	−203.3	−17.8	−21.0	−145.5	−8.7	−13.5
	→	$[Al(O_2^{\bullet})(H_2O)_5]^{2+} + OH^-$	30.5	13.5	11.6			
$[Al(OH)_2(H_2O)_4]^{+} + O_2^{\bullet -}$	→	$Al(O_2^{\bullet})(OH)_2(H_2O)_3 + H_2O$	−100.7	−7.7	−10.0	−75.2	−1.7	−2.8
	→	$[Al(O_2{\bullet}(OH)(H_2O)_4]^{+} + OH^-$	21.8	11.8	7.8			
$Al(OH)_3(H_2O)_2 + O_2^{\bullet -}$	→	$[Al(O_2^{\bullet})(OH)_3(H_2O)]^{-} + H_2O$	−23.0	−15.5	−17.1	−14.6	−2.0	−1.8
	→	$Al(O_2^{\bullet})(OH)_2(H_2O)_3 + OH^-$	17.6	12.3	6.8			
$[Al(OH)_4]^{-} + O_2^{\bullet -}$	→	$[Al(O_2^{\bullet})(OH)_3]^{-} + OH^-$	13.5	13.9	7.8	22.4	15.8	11.2

[a] For the calculation of the energy of $OH_2/OH^-/O_2^{\bullet -}$ species, two explicit water molecules are added in the calculations to reduce errors associated with solvation (see section 3C1).

2. Substitution Reaction Energies. Reaction free energies for the substitution reactions of one OH^-/H_2O ligand by a $O_2^{\bullet -}$ superoxide can be found in Table 7. As starting structures, we have considered a number of Al(III) hydrolysis species dominant at different pH's, that is, $Al(H_2O)_6^{3+}$ for pH < 5.0, $Al(OH)_4^-$ for pH > 6.2, and $Al(OH)(H_2O)_5^{2+}$, *trans*-$Al(OH)_2(H_2O)_4^+$, and *trans*-$Al(OH)_3(H_2O)_3$ for intermediate pH's. On the basis of the most stable structures found by Yang et al.,[14] we substitute one OH^-/H_2O by a superoxide molecule. In order to introduce the smaller number of changes on the solvation shell around Al(III), we first introduced $O_2^{\bullet -}$ in a bent monodentate interaction mode, which maintains the coordination number around Al^{3+}. All of these structures were stable, although further stabilization could be obtained by adopting a T-shape interaction mode with displacement of additional water molecules from the first solvation sphere. However, the initial stages of Al^{3+} superoxide formation should probably proceed through substitution of a single OH^-/H_2O ligand, with preservation of the rest of the solvation sphere, and therefore, these structures are reliable indicators of the different affinities and trends of Al(III) hydrolytic species toward Al^{3+} superoxide formation.

In the gas phase, the substitution reaction of a water molecule by superoxide is highly favorable for any of the complexes, with the affinity decreasing as the number of hydroxides around Al^{3+} increases, $Al(H_2O)_6^{3+}$ (−288.1) > $Al(OH)(H_2O)_5^{2+}$ (−203.3) > $Al(OH)_2(H_2O)_4^+$ (−100.7) > $Al(OH)_3(H_2O)_3$ (−23.0), with the numbers in parentheses corresponding to ΔG values in kcal/mol. In contrast, gas-phase hydroxide substitution shows an endoergonic behavior, less endoergonic as the number of hydroxides decreases, $Al(OH)_4^-$ (13.5) > $Al(OH)_3(H_2O)_3$ (17.6) > $Al(OH)_2(H_2O)_4^+$ (21.8) > $Al(OH)(H_2O)_5^{2+}$ (30.5). Bulk solvent effects are more important for water substitution reactions than for hydroxide ones because in the former, there is a reduction of the total charge of the Al(III) species upon Al(III) superoxide formation. Bulk solvent effects reduce the exoergonicity of water substitution reactions and decrease the endoergonicity of hydroxide substitution, although the effect is lower in this latter case. Still, after introduction of bulk solvent effects, Al(III) superoxide formation is exoergonic for water substitution and endoergonic for hydroxide substitution.

To assess the reliability of our models, we have also examined the influence of a second solvation sphere in the case of water substitution reactions and for the hydroxide substitution reaction in $Al(OH)_4^-$ (see Figure 2). The addition of this second solvation layer, composed of 12 additional water molecules, has been claimed to be fundamental to treat properly the short-range interaction between Al^{3+} and the solvent.[14,22] The addition of these second-shell water molecules does not alter the exoergonicity of these reactions, with $Al(H_2O)_6^{3+}$ (−8.3/−15.2) and $Al(OH)(H_2O)_5^{2+}$ (−8.7/−13.5) structures showing clearly the highest affinity (in parentheses are values of $\Delta G_{aq}^{SMD}/\Delta G_{aq}^{PCM}$, in kcal/mol) and $Al(OH)_2(H_2O)_4^+$ (−1.7/−2.8) > $Al(OH)_3(H_2O)_3$ (−2.0/−1.8) showing the lowest. As in the gas phase, there is an inverse correlation between the number of hydroxides in the first coordination shell and superoxide affinity. On the other hand, there is still a strong thermodynamic penalty for Al(III) superoxide formation via hydroxide substitution in $Al(OH)_4^-$ (15.8/11.2). Our results imply that the formation of an Al(III) superoxide complex in solution can take place by displacement of a water molecule of the first solvation shell, and taking into account the affinities of the different Al(III) species and the distribution of soluble aluminum hydrolytic species, we conclude that Al^{3+} complexation with superoxide is the main path toward Al(III) superoxide formation.

D. Interpretation of the Results. Since the seminal work of Kong et al.,[24] in which it was demonstrated that Al(III) augments the oxidation rate of reduced nicotinamide adenine dinucleotide, there has been an increasing interest in determining the mechanism of the pro-oxidant activity of aluminum. As this early work suggested, the formation of an Al(III) complex with $O_2^{\bullet -}$ could be at the center of this oxidant activity because the presence of superoxide dismutase inhibited the action of Al(III). Since then, the published open literature work[25,26] has provided with

dx.doi.org/10.1021/jp203290b |J. Phys. Chem. A 2011, 115, 6717–6723

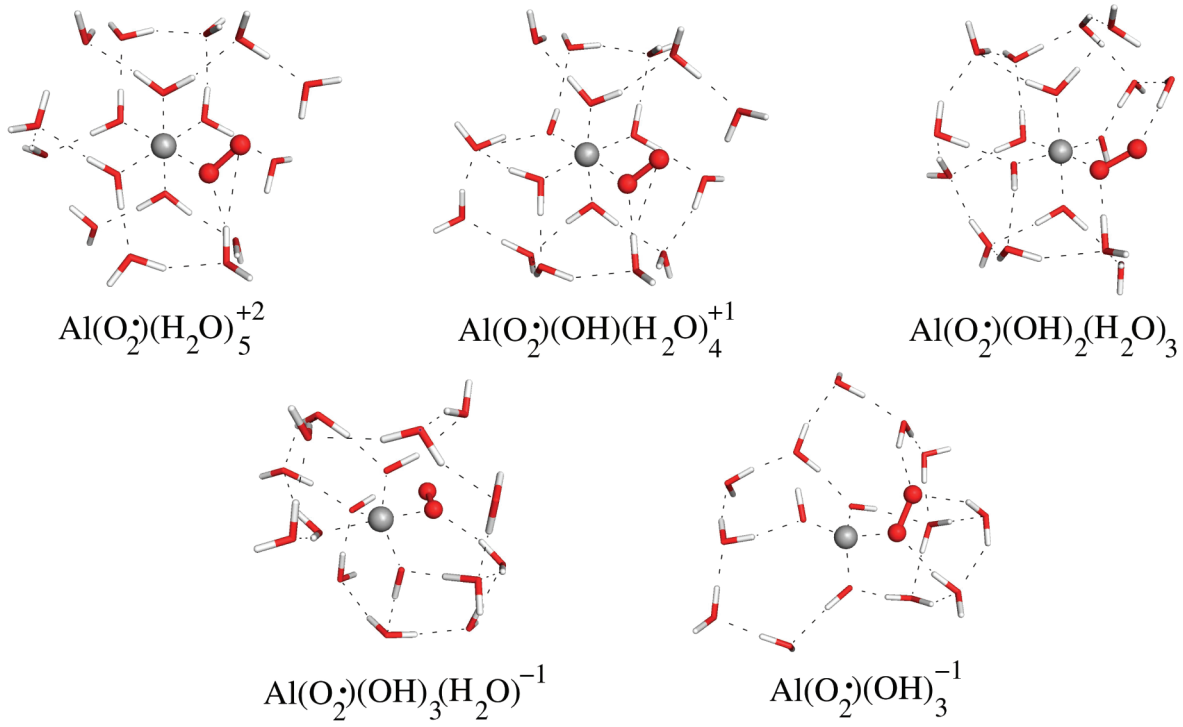

Figure 2. Model of Al^{3+} superoxide species including explicit first and second solvation spheres, structures optimized at the B3LYP/6-31++G(d,p) level of theory.

significant but still circumstantial evidence for the existence of an aluminum superoxide semireduced radical ion. Our characterized **g**-tensor values and the splitting of the π_g levels in $O_2^{\bullet-}$ upon aluminum interaction reveal an intrinsic high capacity of Al^{3+} for superoxide stabilization, much higher than metals such as Mg^{2+} that are prone to exchange with Al^{3+}. Taking into account the linear relationship between metal−superoxide interaction strength and promoting effects in electron-transfer reactions for other metals,[27−29] our results give support to the hypothesis that aluminum constitutes an important pro-oxidant agent in biological systems.

Our present calculations strongly support the existence of an Al(III) superoxide complex in solution via its interaction with Al^{3+} species, rather than via $Al(OH)_4^-$. This latter form of aluminum, which has a much higher concentration at physiological pH, is biologically irrelevant because it does not bind to ligands or proteins in aqueous media.[3,4] The strong affinities and exoergonicity of Al^{3+} toward the superoxide suggest that even small concentrations of Al^{3+} free species would be relevant for oxidant activity, as was previously suggested.[26] In addition, the presence of LMM ligands such as citrate could also have an indirect effect in the oxidation capacity of aluminum by augmenting the bioavailability of Al^{3+} species, shifting the formation of $Al(OH)_4^-$ to higher pH's. However, one should also take into account the effect of citrate chelation itself in the thermodynamic equilibrium of $[AlO_2^{\bullet}]^{2+}$ formation.

Once an $[AlO_2^{\bullet}]^{2+}$ species is formed, how this radical ion leads to oxidative damage is still speculative. Several possibilities could coexist. For instance, it has been reported[25] that a significant concentration of Al(III) potentiates the Fe(II)/Fe(III) redox cycle in favor of Fe(II), supporting the notion that oxidative damage may be the result of Fenton chemistry promoted by the presence of Al(III). On the other hand, other routes are also possible because aluminum also facilitates non-iron-mediated formation of hydroxyl radical.[57] The evaluation of all these various possibilities through the determination of accurate thermodynamics in the presence of $[AlO_2^{\bullet}]^{2+}$ species will be the subject of future work.

4. CONCLUSIONS

The mechanism which underlies the pro-oxidant activity of aluminum remains to be fully elucidated. However, the formation of an aluminum superoxide semireduced radical anion $(O_2^{\bullet-})$ is the only suggested mechanism that explains aluminum-mediated catalysis of both iron- and non-iron-driven biological oxidation, and it is a mechanism for which there is indirect evidence of the existence of such a species.[25,26] We now present the first computational evidence of the strong likelihood of the existence of this redox-active species in physiological media and its putative role in the known pro-oxidant activity of aluminum. Our calculations point to the formation of an $[AlO_2^{\bullet}]^{2+}$ by displacement of a water molecule in $[Al(H_2O)_6]^{3+}$ species rather than hydroxide displacement in $[Al(OH)_4]^-$, emphasizing the biological importance of the concentration of the Al^{3+} free form.

■ ASSOCIATED CONTENT

Supporting Information. Comparison between reaction energies. This material is available free of charge via the Internet at http://pubs.acs.org.

■ ACKNOWLEDGMENT

Financial support comes from Eusko Jaurlaritza and the Spanish Office for Scientific Research. The SGI/IZO−SGIker UPV/EHU is gratefully acknowledged for generous allocation of computational resources.

REFERENCES

(1) Exley, C. *J. Inorg. Biochem.* **2003**, *97*, 1–7.
(2) Exley, C. *Trends Biochem. Sci.* **2009**, *34*, 589–593.
(3) Martin, R. *Acc. Chem. Res.* **1994**, *27*, 204–210.
(4) MacDonald, T.; Martin, R. *Trends Biochem. Sci.* **1988**, *13*, 15–19.
(5) Bharathi.; Vasudevaraju, P.; Govindaraju, M.; Palanisamy, A.; Sambamurti, K.; Rao, K. *Indian J. Med. Res.* **2008**, *128*, 545–556.
(6) Tomljenovic, L. *J. Alzheimers Dis.* **2011**, *23*, 567–598.
(7) Murko, S.; Milačič, R.; Ščančar, J. *J. Inorg. Biochem.* **2007**, *101*, 1234–1241.
(8) Aquino, A. J. A.; Tunega, D.; Haberhauer, G.; Gerzabek, M. H.; Lischka, H. *Phys. Chem. Chem. Phys.* **2001**, *3*, 1979–1985.
(9) Oliveira de Noronha, A. L.; Guimaraes, L.; Duarte, H.A. *J. Chem. Theory Comput.* **2007**, *3*, 930–937.
(10) Swaddle, T. W.; Rosenqvist, J.; Yu, P.; Bylaska, E.; Phillips, B. L.; Casey, W. H. *Science* **2005**, *308*, 1450–1453.
(11) Rezabal, E.; Mercero, J. M.; Lopez, X.; Ugalde, J. M. *J. Inorg. Biochem.* **2006**, *100* (3), 374–384.
(12) Rezabal, E.; Mercero, J. M.; Lopez, X.; Ugalde, J. M. *ChemPhysChem* **2007**, *8*, 2119–2124.
(13) Rezabal, E.; Mercero, J. M.; Lopez, X.; Ugalde, J. M. *J. Inorg. Biochem.* **2007**, *101* (9), 1192–1200.
(14) Yang, W.; Qian, Z.; Miao, Q.; Wang, Y.; Bi, S. *Phys. Chem. Chem. Phys.* **2009**, *11* (14), 2396–2401.
(15) Fan, J. F.; He, L. J.; Liu, J.; Tang, M. *J. Mol. Model.* **2010**, *16*, 1639–1650.
(16) Lubin, M. I.; Bylaska, E. J.; Weare, J. H. *Chem. Phys. Lett.* **2000**, *322* (6), 447–453.
(17) Sillanpää, A.; Päivärinta, J.; Hotokka, M.; Rosenholm, J.; Laasonen, K. *J. Phys. Chem. A* **2001**, *105*, 10111–10122.
(18) Hay, M. B.; Myneni, S. C. B. *J. Phys. Chem. A* **2008**, *112*, 10595–10603.
(19) Lu, B.-M.; Jin, X.-Y.; Tang, J.; Bi, S.-P. *J. Mol. Struct.* **2010**, *982* (1−3), 9–15.
(20) Beardmore, J.; Rugg, G.; Exley, C. *J. Inorg. Biochem.* **2007**, *101*, 1187–1191.
(21) Beardmore, J.; Exley, C. *J. Inorg. Biochem.* **2009**, *103*, 205–209.
(22) Mujika, J.; Ugalde, J.; Lopez, X. *Theor. Chem. Acc.* **2011**, *128*, 477–484.
(23) Dudev, T.; Lim, C. *Annu. Rev. Biophys.* **2008**, *37*, 97–116.
(24) Kong, S.; Liochev, S.; Fridovich, I. *Free Radical Biol. Med.* **1992**, *13*, 79–81.
(25) Khan, A.; Dobson, J.; Exley, C. *Free Radical Biol. Med.* **2006**, *40*, 557–569.
(26) Exley, C. *Free Radical Biol. Med.* **2004**, *36* (2), 380–387.
(27) Fukuzumi, S.; Ohkubo, K. *Chem.—Eur. J.* **2000**, *6*, 4532–4535.
(28) Fukuzumi, S. *J. Phys. Org. Chem.* **2002**, *15*, 448–460.
(29) Fukuzumi, S.; Ohtsu, H.; Ohkubo, K.; Itoh, S.; Imahori, H. *Coord. Chem. Rev.* **2002**, *226*, 71–80.
(30) Frisch, M. J.; Trucks, G. W.; Schlegel, H. B.; Scuseria, G. E.; Robb, M. A.; Cheeseman, J. R.; Scalmani, G.; Barone, V.; Mennucci, B.; Petersson, G. A.; Nakatsuji, H.; Caricato, M.; Li, X.; Hratchian, H. P.; Izmaylov, A. F.; Bloino, J.; Zheng, G.; Sonnenberg, J. L.; Hada, M.; Ehara, M.; Toyota, K.; Fukuda, R.; Hasegawa, J.; Ishida, M.; Nakajima, T.; Honda, Y.; Kitao, O.; Nakai, H.; Vreven, T.; Montgomery, J. A., Jr.; Peralta, P. E.; Ogliaro, F.; Bearpark, M.; Heyd, J. J.; Brothers, E.; Kudin, K. N.; Staroverov, V. N.; Kobayashi, R.; Normand, J.; Raghavachari, K.; Rendell, A.; Burant, J. C.; Iyengar, S. S.; Tomasi, J.; Cossi, M.; Rega, N.; Millam, N. J.; Klene, M.; Knox, J. E.; Cross, J. B.; Bakken, V.; Adamo, C.; Jaramillo, J.; Gomperts, R.; Stratmann, R. E.; Yazyev, O.; Austin, A. J.; Cammi, R.; Pomelli, C.; Ochterski, J. W.; Martin, R. L.; Morokuma, K.; Zakrzewski, V. G.; Voth, G. A.; Salvador, P.; Dannenberg, J. J.; Dapprich, S.; Daniels, A. D.; Farkas, Ö.; Ortiz, J. V.; Cioslowski, J.; Fox, D. J. *Gaussian 09*, revision A.1; Gaussian, Inc.: Wallingford, CT, 2009.
(31) Becke, A. D. *J. Chem. Phys.* **1993**, *98*, 5648–5652.
(32) Becke, A. D. *Phys. Rev. A* **1988**, *38*, 3098–3100.
(33) Lee, C.; Yang, W.; Parr, R. G. *Phys. Rev. B* **1988**, *37*, 785–789.
(34) Vosko, S. H.; Wilk, L.; Nusair, M. *Can. J. Phys.* **1980**, *58* (8), 1200–1211.
(35) Adamo, C; Varone, V. *J. Chem. Phys.* **1999**, *110*, 6158.
(36) Zhao, Y.; Truhlar, D. G. *Theor. Chem. Acc.* **2008**, *120*, 215.
(37) Douglas, M.; Kroll, N. M. *Ann. Phys. (N.Y.)* **1974**, *82*, 89.
(38) Hess, B. A. *Phys. Rev. A* **1986**, *33*, 3742.
(39) Roos, B. O.; Taylor, P. R.; Siegbahn, P. E. M. *Chem. Phys.* **1980**, *48*, 157.
(40) Siegbahn, P. E. M.; Heiberg, A.; Roos, B. O.; Levy, B. *Phys. Scr.* **1980**, *21*, 323.
(41) Siegbahn, P. E. M.; Almlöf, J.; Heiberg, A.; Roos, B. O. *J. Chem. Phys.* **1981**, *74*, 2384.
(42) Andersson, K.; Malmqvist, P.-Å.; Roos, B. O.; Sadlej, A. J.; Wolinski, K. *J. Phys. Chem.* **1990**, *94*, 5483.
(43) Andersson, K.; Malmqvist., P.-Å.; Roos., B. O. *J. Chem. Phys.* **1992**, *96*, 1218.
(44) Forsberg., N.; Malmqvist., P.-Å. *Chem. Phys. Lett.* **1997**, *274*, 196.
(45) Aquilante, F.; De Vico, L.; Ferré, N.; Ghigo, G.; Malmqvist, P.-A.; Neogrády, P.; Pedersen, T. B.; Pitoňák, M.; Reiher, M.; Roos, B. O.; Serrano-Andrés, L.; Urban, M.; Veryazov, V.; Lindh, R. *J. Comput. Chem.* **2010**, *31*, 224.
(46) Vancoillie, S.; Malmqvist., P.-Å.; Pierloot, K. *ChemPhysChem* **2007**, *8*, 1803.
(47) Roos, B. O.; Lindh, R.; Malmqvist., P.-Å.; Veryazov, V. *J. Phys. Chem. A* **2005**, *108*, 2851.
(48) Roos, B. O.; Veryazov, V.; Widmark, P.-O. *Theor. Chem. Acc.* **2005**, *111*, 345.
(49) Widmark, P.-O.; Malmqvist., P.-Å.; Roos, B. O. *Theor. Chim. Acta* **1990**, *77*, 291.
(50) Barone, V.; Cossi, M.; Tomasi, J. *J. Comput. Chem.* **1998**, *19*, 404–417.
(51) Barone, V.; Cossi, M.; Tomasi, J. *J. Chem. Phys.* **1997**, *107*, 3210–3221.
(52) Cossi, M.; Barone, V.; Cammi, R.; Tomasi, J. *Chem. Phys. Lett.* **1996**, *255*, 327–335.
(53) Cances, E.; Mennucci, B.; Tomasi, J. *J. Chem. Phys.* **1997**, *107*, 3032–3041.
(54) Marenich, A. V.; Cramer, C. J.; Truhlar, D. G. *J. Phys. Chem. B* **2009**, *113*, 6378–6396.
(55) Pliego, J. R., Jr.; Riveros, J. M. *Phys. Chem. Chem. Phys.* **2002**, *4*, 1622–1627.
(56) Takano, Y.; Houk, K. N. *J. Chem. Theory Comput.* **2005**, *1*, 70–77.
(57) Mendez-Alvarez, E.; Soto-Otero, R.; Hermida-Ameijeiras, A.; Lopez-Real, A.; Labandeira-Garcia, J. L. *Biochim. Biophys. Acta* **2002**, *1586*, 155–168.